J. Fluid Mech. (1980), *vol.* 101, *part* 2, *pp.* 307–319
Printed in Great Britain

Shock detachment from cones in a relaxing gas

By H. G. HORNUNG† AND A. F. P. HOUWING
Department of Physics, Australian National University, Canberra, Australia

(Received 8 November 1979)

Measurements of the shock stand-off distance on cones of various base diameters in carbon dioxide and nitrogen flows with dissociative relaxation show that the detachment process occurs more gradually with relaxation than in a perfect gas, as the cone semi-angle is increased. This is in agreement with a prediction which is made on the basis of the behaviour of the sonic surface in the flow field. The phenomenon is similar to that observed previously with wedge flow but shows interesting effects peculiar to the cone flow. The cone experiments also eliminate the end effect and permit easy variation of the relaxation rate parameter without changing the gas. Perfect-gas argon experiments provide a convenient check.

1. Introduction

This paper is concerned with the inviscid, high-Mach-number flow of a relaxing gas over cones at zero incidence with semi-angles in the range around the value at which the shock wave detaches from the cone tip. The shock is taken to be partly dispersed, the situation of particular interest being that in which a translational–rotational subshock of unresolvably small thickness is followed by a region of vibrational and dissociative relaxation, the extent of which is characterized by a single relaxation length, l.

Whether an observer sees such a flow to be in thermodynamic equilibrium or not depends on the relative magnitudes of his smallest resolvable length scale λ, his largest viewable length Λ, and the relaxation length l. If he cannot resolve l, or if

$$l < \lambda < \Lambda, \tag{1}$$

an equilibrium exists, while, if

$$\lambda < l < \Lambda, \tag{2}$$

the relaxation is resolvable and must therefore be taken into account. At the other extreme, when

$$\lambda < \Lambda \ll l, \tag{3}$$

a 'frozen' situation exists. The gas may be considered to be in a constrained state of equilibrium, which differs from the unconstrained equilibrium state indicated by (1). Hence the equation of state is different for case (3) than for case (1). Since the conditions after a plane oblique shock are determined from the free-stream conditions by the conservation and state equations, they will be different for (1) and (3), and, in case (2) the conditions after the translational shock are as for (3) while they asymptotically approach those specified by (1) further from the shock.

The conditions achievable from a free-stream state, A, by a plane, oblique shock may be conveniently presented in the speed–deflexion (V–δ) plane, see figure 1. The two

† Present address: DFVLR-AVA, 34 Göttingen, Bunsenstr. 10, W. Germany.

0022-1120/80/4578-2430 $02.00

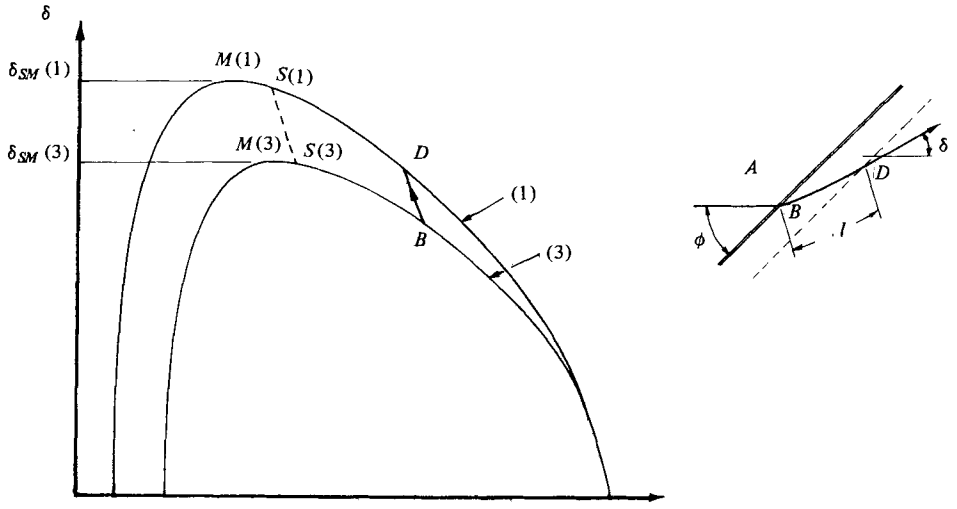

FIGURE 1. Shock loci in the speed–deflexion plane for equilibrium (1) and frozen (3) flow. – – – –, sonic line relative to frozen speed of sound.

curves represent the loci of conditions after the shock as observed in cases (1) and (3) respectively as the shock strength is increased from zero at point A. The maximum deflexion points $M(3)$ and $M(1)$ represent the largest angles of a wedge at which an attached shock can be observed in the respective situations. For high free-stream Mach number, the point $S(3)$ at which the flow is sonic (flow speed = frozen speed of sound) at the sub-shock practically coincides with $M(3)$.

By considering the flow over a wedge of angle δ_w such that

$$\delta_{SM}(3) < \delta_w < \delta_{SM}(1), \tag{4}$$

Hornung & Smith (1979) showed that, in this range, the shock stand-off distance, Δ, is $O(l)$, and that Δ increases more gradually with relaxation than for a perfect gas. They related this behaviour to the phenomenon that, as ϕ is increased beyond a certain value, a subsonic layer starts to grow from the subshock into the relaxation layer while the flow further downstream is still supersonic. Their experiments with dissociating nitrogen and carbon dioxide flows substantiated these predictions and were given additional weight by being contrasted with a perfect-gas argon experiment.

One of the weaknesses of wedge flow experiments is that the transverse length of the wedge is finite. The end effects influence results in a similar way as relaxation does, and a null-experiment with a perfect gas becomes essential. One of the motivations for repeating the experiments with cones was that the end effect is automatically removed in axisymmetric flow. The relative ease of making cones also allows the important parameter l/d to be varied without changing the gas by making cones of different base diameter, d.

2. Relaxing cone flow

2.1. *Weak and strong relaxation*

The flow over cones is more complex than wedge flow, as the condition at the body, characterized for example by the cone semi-angle δ_C, is not the same as that at the

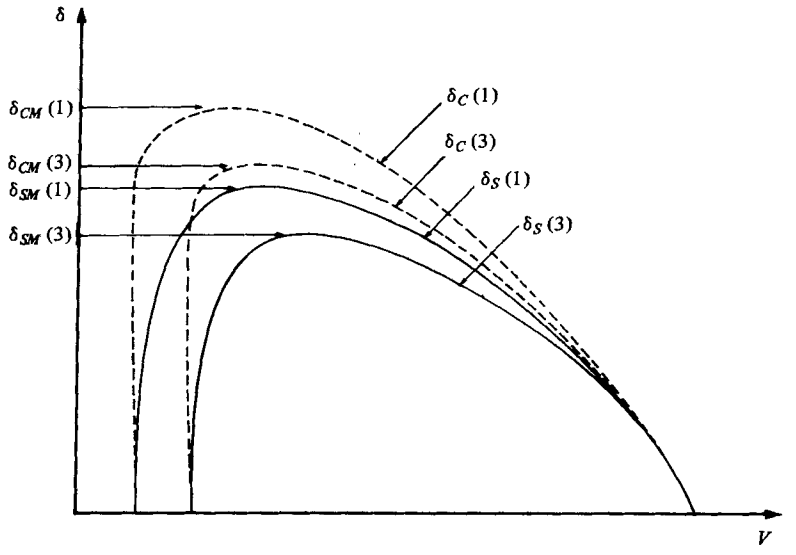

FIGURE 2. Shock and body loci for frozen (3) and equilibrium (1) cone flow in the case of weak relaxation, $\delta_{SM}(1) < \delta_{CM}(3)$.

shock, δ_S, even in equilibrium or frozen flow. The conditions at the body map into a body locus in the V–δ plane, the shock detachment condition being given by

$$\delta_C = \delta_{CM}, \tag{5}$$

where δ_{CM} is the extreme value of δ_C. Again, the body locus for the frozen situation (3) is different from that for the equilibrium situation (1), as is the case for the shock locus. One may now distinguish between two cases according to the relative magnitude of the extreme deflexion angles at the shock and cone in the frozen and equilibrium situations. We denote by 'strong' and 'weak' relaxation the cases when $\delta_{SM}(1)$ is greater or less than $\delta_{CM}(3)$ respectively. The V–δ map of the case of weak relaxation is shown in figure 2.

This is the case relevant to the present discussion and, indeed, strong relaxation may be expected to be quite rare in a laboratory environment. This can be demonstrated by the following simple estimate. Numerical solutions of the equations of perfect gas cone flow give δ_{CM} as a function of γ, the ratio of specific heats. The values of δ_{CM} and the corresponding maximum deflexion at the shock are shown in figure 3 for infinite free-stream Mach number. Taking the case of a free stream of diatomic molecules, $\gamma = 1{\cdot}4$, and figure 3 gives $\delta_{CM}(3) \simeq 57°$. The curve for δ_{SM} has this value at $\gamma = 1{\cdot}18$. For $\delta_{CM}(3) = \delta_{SM}(1)$, the internal degrees of freedom of the equilibrium flow would have to use up enough energy to make the effective ratio of specific heats equal to 1·18, corresponding to a hypersonic density ratio across the shock of 12·1. While this is possible in free flight, it is unusual in wind-tunnel experiments, because freezing of the internal degrees of freedom in the nozzle flow invariably causes the free stream to remain partially dissociated. In the free-piston shock tunnel a density ratio of 12 in nitrogen has only been achieved across a normal shock. In the following, we shall therefore restrict discussion to the case of weak relaxation.

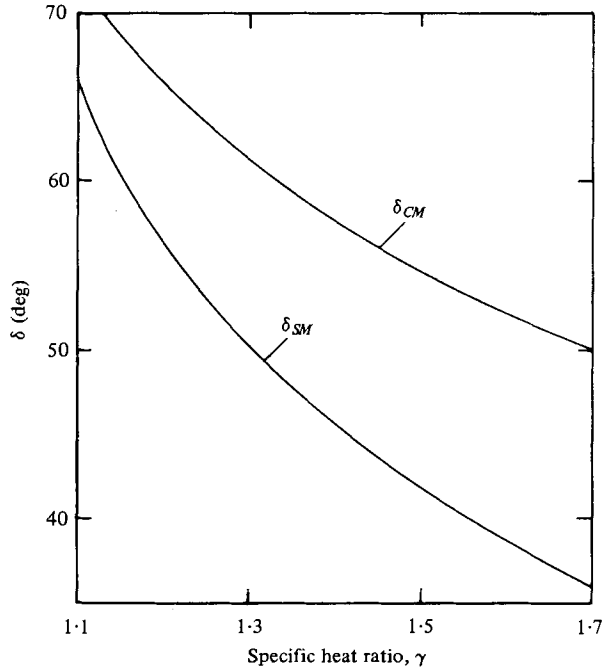

FIGURE 3. Calculated maximum deflexion angles at the shock and at the cone in perfect-gas flow at infinite free-stream Mach number.

2.2. *The V–δ map of cone flow with an attached shock*

When the cone angle is sufficiently small, the shock is attached to the cone tip and the flow is everywhere supersonic. Within a distance $\Lambda(3)$ of the cone tip, such that $\Lambda(3) \ll l$, the frozen conditions apply. Consider first the streamline that passes through the shock very close to the tip. It suffers an initial discontinuous deflexion to $\delta_S(3)$ at the shock, followed by a further deflexion asymptotically approaching the cone semi-angle δ_C. During this second continuous deflexion the velocity decreases along the streamline according to a relation $\delta(V)$ which can be determined from numerical solutions of frozen cone flow. Since $\Lambda(3) \ll l$, no appreciable relaxation takes place along this streamline until it has reached the cone semi-angle δ_C on the body locus $\delta_C(3)$. The subsequent relaxation along this streamline occurs at constant deflexion and is accompanied by an increase in velocity, so that the conditions on it finally approach a point close to $\delta_C = \delta_C(1)$ in the V–δ plane. This streamline is shown in figure 4(*b*) in the physical plane as BC, and its corresponding V–δ map is $BB'C$ in figure 4(*a*). Note that the point B in the physical plane maps into the line BB' in the V–δ plane.

The streamline that passes through the shock at a distance from the tip much larger than the relaxation length, l, must approach the point $\delta_C = \delta_C(1)$ eventually. It is shown as DEF in figure 4(*b*). The distance measured along this streamline to the point where the flow deflexion approaches the body deflexion δ_C is large compared with l. The deflexion of the streamline due to relaxation is therefore completed before any significant turning due to the cone flow occurs. The V–δ map of this equilibrium streamline is also shown in figure 4(*a*). Clearly, the curves BB' and EF represent the frozen and equilibrium cone flow solutions respectively for a cone of semiangle δ_C.

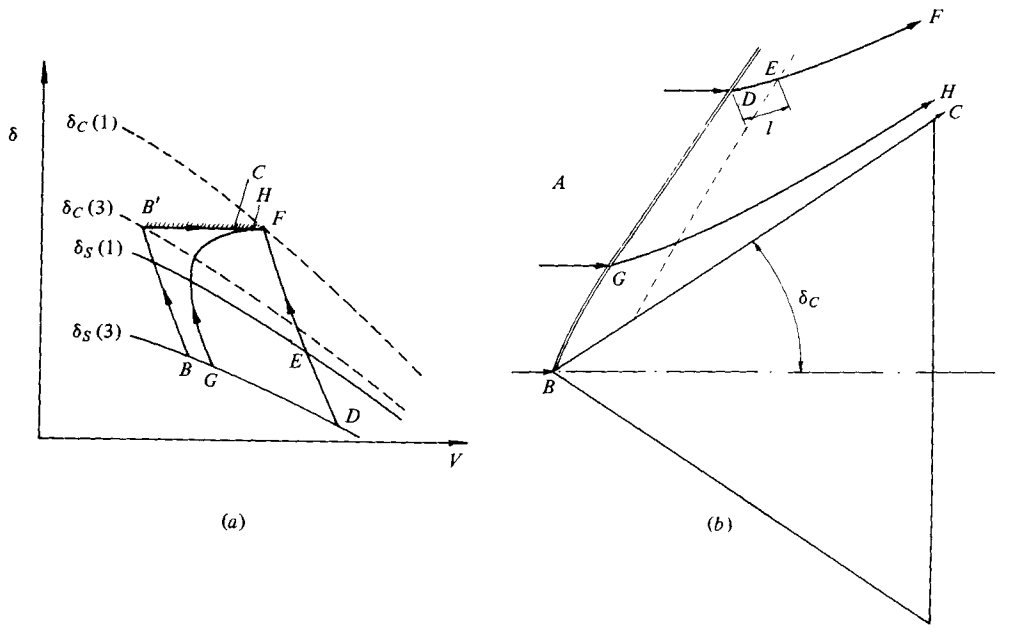

FIGURE 4. Relaxing flow over a cone with attached shock and supersonic conditions throughout. (*a*) V–δ plane; (*b*) physical plane.

The V–δ map now shows that the translational subshock must be curved between B and D. Since the body loci $\delta_C(3)$, $\delta_C(1)$ as well as the equilibrium shock locus $\delta_S(1)$ only apply for straight shocks, they can only be used for the frozen and equilibrium extremes in the cone flow. However, the qualitative behaviour of the V–δ map of a streamline through a curved shock has been determined by Hornung (1977) for the plane case, and the results may be easily extended to axisymmetric flows. Applied to the present problem they yield the qualitative shape of the V–δ map of the general streamline GH shown in figure 4. Note, that the intersections of this streamline with the lines $\delta_S(1)$ and $\delta_C(3)$ have lost their significance because the shock radius of curvature at G is neither very large nor very small compared with l. The separation of the asymptotic points C and F in the V–δ plane also arises from the fact that the shock angles at B and D are not the same so that, though the asymptotic pressures at C and F are the same, the streamline near the body has a higher entropy and therefore a lower velocity.

2.3. *The sonic line*

Since we have only considered the supersonic problem so far, the size of the cone was not important. As the cone semiangle δ_C is increased, however, the flow becomes locally subsonic. The existence of subsonic regions provides the mechanism by which the detachment process derives its length scale either from the relaxation length or from the size of the cone. The latter may conveniently be specified by the base diameter, d.

Consider first the case of perfect-gas (frozen) flow. The equations of cone flow admit conical solutions in which both subsonic and supersonic regions occur, the conical sonic surface separating a subsonic region near the body from a supersonic one near the shock. If the cone is finite, this provides a path by which the trailing edge of the cone

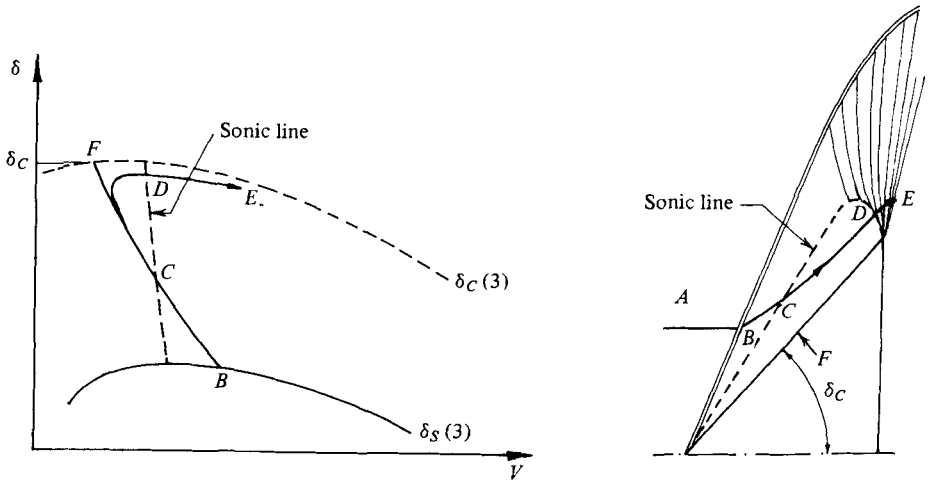

FIGURE 5. Mixed (supersonic and subsonic) cone flow of a perfect gas.

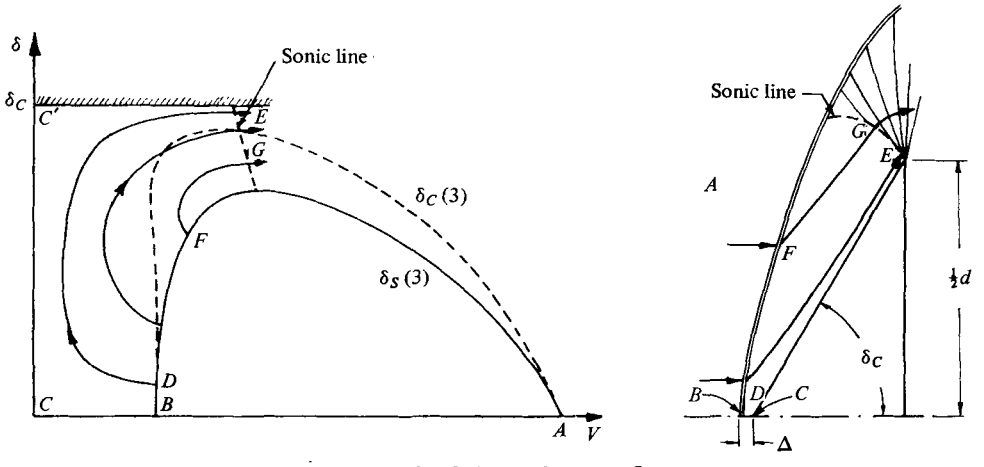

FIGURE 6. Detached shock in perfect-gas flow over a cone.

can influence the flow near the tip. However, it appears that, at least for a small range of angles, this is not enough to cause the shock to be influenced (see Solomon 1955). The sonic line has to meet the trailing edge where the flow is accelerated by the corner. The mixed case for perfect gas flow over a finite cone with its V–δ map is shown schematically in figure 5.

The cone angle for maximum deflexion is somewhat larger than that for a sonic shock. Thus when the cone semiangle has reached $\delta_{CM}(3)$ conditions behind the shock are already subsonic. The trailing edge of the cone, and therefore the length scale d, can influence the shock, so that the shock is curved. For cone angles larger than $\delta_{CM}(3)$ the shock detaches. The detachment distance, Δ, increases approximately linearly with $\delta_C - \delta_{CM}(3)$ (see Ward & Pugh 1968). The detached flow and its V–δ map are shown in figure 6. Clearly, the body locus in the V–δ plane no longer has any significance in this case because the shock is curved. Similarly, the shape of the sonic line in the V–δ plane depends on the shock shape in the physical plane, though its end point on the shock is fixed.

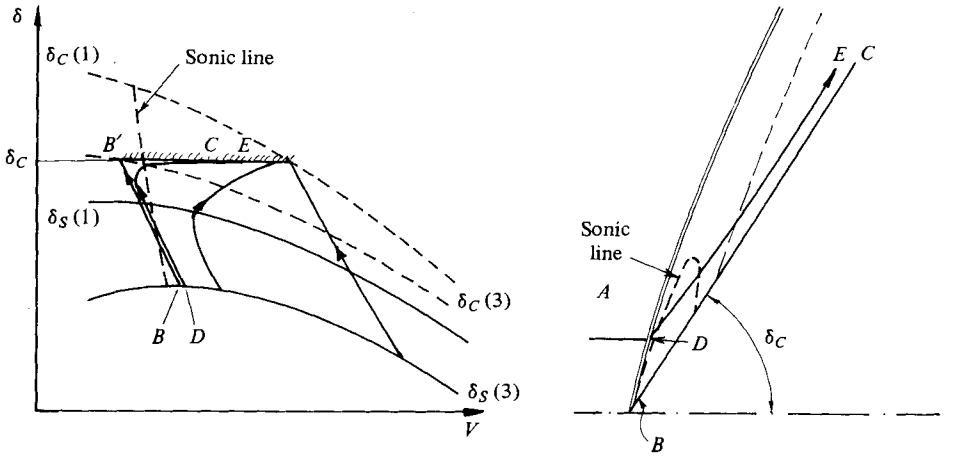

FIGURE 7. Relaxing cone flow. Attached shock, subsonic region embedded in relaxation region.

Now introduce relaxation and, for simplicity, take the case $d \gg l$ first. Consider the attached shock of figure 4 and let δ_C be increased, so that the 'quadrilateral' enclosing the flow field in the V–δ plane slides up and to the left, its corners being constrained to lie on $\delta_C(1)$, $\delta_C(3)$ and $\delta_S(3)$. As δ_C is increased, there comes a point at which B' crosses the sonic line. However, the Mach number on the streamlines entering the subsonic region is increased again by the relaxation, so that the complete flow picture is as shown in figure 7.

As δ_C is increased to a point where $\delta_C > \delta_{CM}(3)$, the frozen shock detaches, but the detachment distance remains so small that it cannot be resolved by an observer for whom the inequalities (1) apply. This is consistent with the form of the corresponding V–δ map of the flow, see figure 8. It shows that the extent of the subsonic region from which the detachment distance derives its scale is less than the relaxation length l.

Further increase of δ_C causes the extent of the subsonic region to increase further, until it exceeds the relaxation length. This occurs when $\delta_C \simeq \delta_{CM}(1)$. Thereafter the point where the sonic line meets the body lies at the trailing edge of the cone, and the flow picture is qualitatively very similar to that of figure 6. The length scale governing Δ is then the cone size d. The shock stand-off distance Δ may be expected to increase more slowly with δ_C when $\delta_{CM}(3) < \delta_C < \delta_{CM}(1)$ than when $\delta_C > \delta_{CM}(1)$, since the length scale governing Δ in l is the former range while it is d in the latter.

Now let $d \simeq l$. Consider the case $\delta_{CM}(3) < \delta_C < \delta_{CM}(1)$. The subsonic region may now be terminated by the expansion around the trailing edge and not by the relaxation. The governing length scale for the detachment distance is then d, so that one may expect only a slight departure from the frozen flow behaviour. If $d \ll l$, figure 6 applies, and Δ is always governed by d. The expected behaviour of Δ/d with δ_C can now be sketched for different values of l/d, see figure 9. This diagram incorporates the linear behaviour of Δ/d with δ_C observed by Ward & Pugh (1968) in the frozen case and assumes that it also occurs at equilibrium. Ward & Pugh's measurements resolve δ_C more finely in the immediate vicinity of detachment than the otherwise more extensive measurements of Emunds (1976).

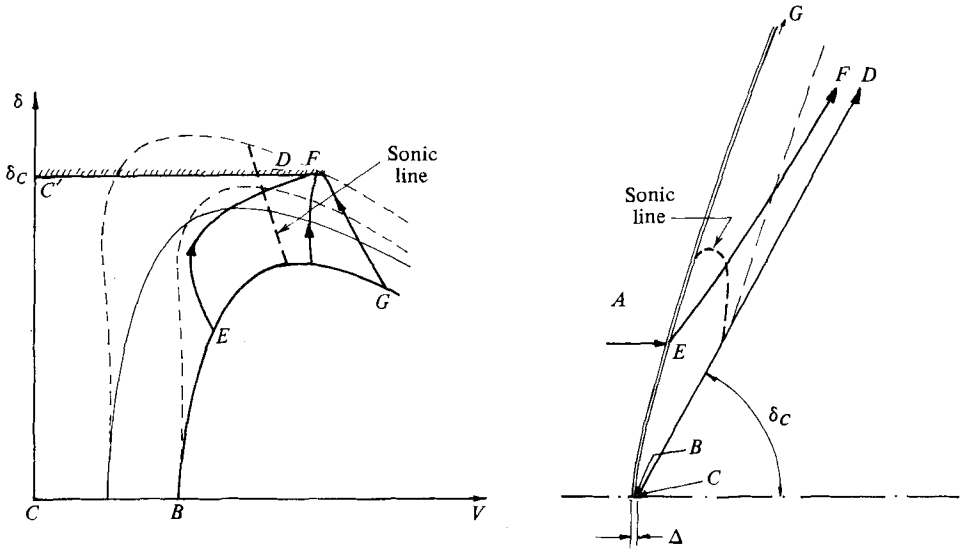

FIGURE 8. Relaxing cone flow. Detached shock, stand-off distance controlled by relaxation length. $\delta_{CM}(3) < \delta_C < \delta_{CM}(1)$. Subsonic region has reached shock.

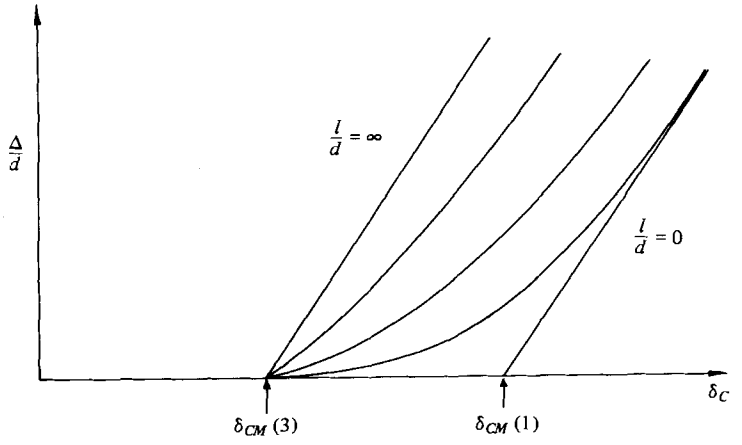

FIGURE 9. Expected behaviour of shock stand-off distance for cones of different sizes relative to the relaxation length.

3. Experiment

3.1. *Facility and free-stream conditions*

The large free-piston shock tunnel was used for all the experiments in the same configuration as in the wedge flow experiments of Hornung & Smith (1979). Mach–Zehnder interferograms were taken of dissociating nitrogen and carbon dioxide flows, and of perfect-gas argon flows. The free-stream conditions of the contoured nozzle flow, calculated numerically from measured reservoir conditions, are given in table 1. The free-stream density in the carbon dioxide and nitrogen flows was increased by a factor of 1·7 over those of the wedge flow experiments in order to reduce the viscous length scale. This has the consequence that the gas composition is slightly changed in favour of the molecular constituents.

	Nitrogen	Carbon dioxide	Argon
Velocity (km s^{-1})	5·2	4·0	2·2
Mach number	7·8	5·9	16
Density (g cm^{-3})	$4{\cdot}3 \times 10^{-6}$	$7{\cdot}8 \times 10^{-6}$	$2{\cdot}2 \times 10^{-6}$
Temperature (K)	1040	1900	57
Composition (mole g^{-1})	N_2 $3{\cdot}37 \times 10^{-2}$ N $4{\cdot}0 \times 10^{-3}$	CO_2 $9{\cdot}1 \times 10^{-3}$ CO $1{\cdot}34 \times 10^{-2}$ O_2 $6{\cdot}2 \times 10^{-3}$ O $1{\cdot}0 \times 10^{-3}$	Ar 0·025

TABLE 1. Free-stream conditions.

3.2. *Range of parameters*

For each of the experimental conditions in table 1, a relation of the form implied by figure 9,

$$\Delta/d = f(l/d, \delta_C) \tag{6}$$

exists for inviscid flow. In the experiment, however, the Reynolds number is finite and is likely to affect the experiment in the case of the smallest cones ($d = 1$ cm), so that the boundary-layer thickness has to be estimated. The case of most interest in the present context is that of incipient detachment of the shock when the Mach number outside the boundary layer, but behind the attached shock, is approximately 1, and conditions outside the boundary layer are uniform. For the small cones, the flow may be assumed to be frozen throughout for the purposes of estimating the boundary-layer displacement thickness, δ^*. For the case of an insulated wall (giving an overestimate of δ^*) the results of van Driest (1952) may be used to obtain

$$\frac{\delta^*}{L} \simeq \frac{2}{\sqrt{Re}} \tag{7}$$

for a flat plate at zero incidence, at sonic conditions outside the boundary layer, for a Prandtl number of 0·75 and a specific heat ratio of 1·4. Though the last two conditions are not exactly satisfied in our experiments, δ^* is not sufficiently sensitive to these parameters to cause concern in our crude estimation. Applying a Mangler transformation to this result to account for the axial symmetry (see, for example, Walz 1966, p. 174), yields

$$\frac{\delta^*}{L} \simeq \frac{2}{\sqrt{3}\sqrt{Re}}. \tag{8}$$

In (7) and (8) L is the length of the generator of the cone, δ^* is the displacement thickness at the trailing edge of the cone, and Re is the Reynolds number outside the boundary layer, based on L.

In both of the dissociating gases the temperature after a frozen shock of 60° incidence to the free stream is approximately 10000 K. Since the wall temperature remains at 300 K during the short test time, the effect of heat transfer to the wall must be considered. This may be estimated by assuming the Prandtl and Lewis numbers to be unity and using equation (8.3.3) of Hayes & Probstein (1959) in a linear velocity

	Nitrogen	Carbon dioxide	Argon
Reynolds number			
L = 1 cm	5000	5000	1500
L = 10 cm	50000	50000	15000
Displacement thickness (cm)			
L = 1 cm	0.005	0·005	0·007
L = 10 cm	0·01	0·01	0·02
Relaxation length l (cm)	1·2	0·4	∞

TABLE 2. Range of boundary-layer displacement thickness at incipient detachment.

profile. In this manner, the effect of wall cooling may be shown to reduce δ^* by a factor of 4. The viscosity may be estimated from data given by Dorrance (1962) to be $(3 \pm 1) \times 10^{-3}$ g cm^{-1} s^{-1} for nitrogen at 10000 K and is assumed to be the same for the carbon-dioxide flow, which consists in a large part of CO. The resulting values of the Reynolds number and estimates of displacement thickness are given in table 2. Clearly, δ^* is near or below the resolution limit. This is in agreement with observation (see, for example, figure 12*d*, near trailing edge).

In the present experiments the parameter l/d was varied both by changing l and by varying the model size d. The dissociation rate is very sensitive to temperature and varies approximately linearly with the density. For a given set of free-stream conditions, the relaxation length is therefore sensitive to the shock angle. Since the range of shock angles of interest to the detachment problem lies in a narrow range around incipient detachment, l may be considered to be constant for each gas. Calculated values of the relaxation length after a normal shock (to where the density change due to relaxation reaches 95 % of its maximum value) are given in the last row of table 2. However, changing l by changing the gas changes the functional form of equation (6) (for example, it changes the values of $\delta_{CM}(1)$ and $\delta_{CM}(3)$) so that this does not help in examining the detailed behaviour predicted by figure 9. It is more profitable to change d. For this purpose a large number of cones was made with a range of semi-angles δ_C and with d = 7·5, 3 and 1 cm. A few very large (d = 15 cm) and very small (d = 0·5 cm) cones were also made, but the limits of the facility size and resolution in interferometry caused results obtained with those to be only of restricted value.

4. Results and discussion

The results of the argon experiments are presented in figure 10. These were all obtained on cones with d = 3 cm. The error bars on the measurement of Δ represent approximately $\pm$ 0·15 mm. Though the photographs permit considerably better resolution, the relatively low density of the argon flow causes the shock in the interferograms to be poorly defined. The behaviour of Δ/d with δ_C can be seen to follow approximately that observed by Ward & Pugh (1968), though there appears to be a slight departure from linearity of the curve in our experiment. As can be seen, the results also agree with the calculated value of δ_{CM}, within the error, though they indicate a slightly higher value.

The results obtained in nitrogen with cones of d = 1, 3 and 7.5 cm are shown in figure 11. It is clear that the error bars on Δ/d, particularly for the small cones, is too large to be able to separate the curve obtained for d = 7·5 cm from that for d = 1 cm

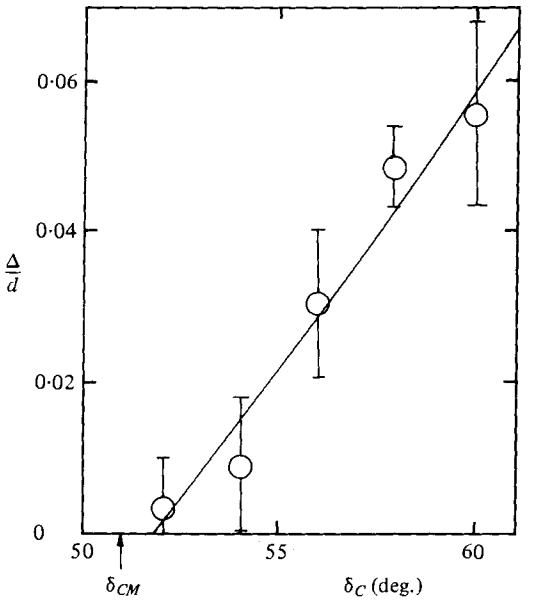

FIGURE 10. Results of perfect-gas argon experiments, $d = 3$ cm. The arrow shows the calculated value of δ_{CM}.

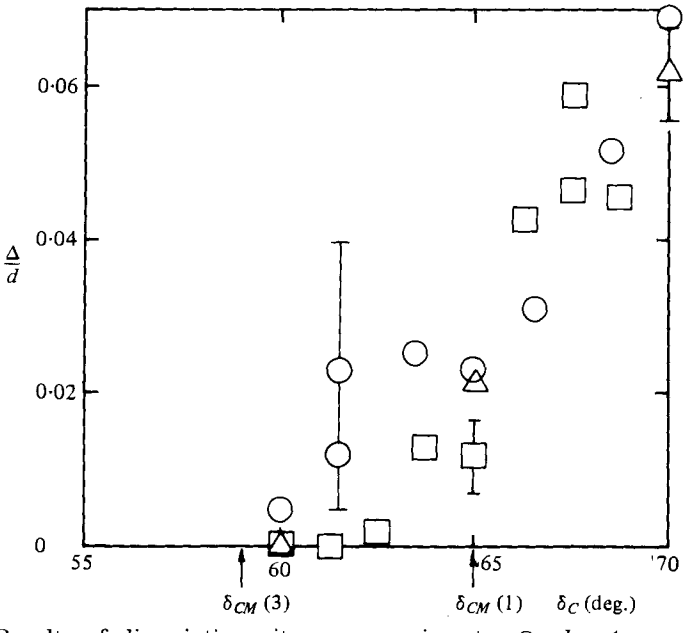

FIGURE 11. Results of dissociating nitrogen experiments. ○, $d = 1$ cm; △, $d = 3$ cm; □, $d = 7{\cdot}5$ cm. The effect of model size is barely significant in view of the measurement errors, Arrows show calculated angles.

with any significance above $\delta_C = 64°$, and it is barely possible to detect the trend predicted by figure 9 below this angle. The calculated values of $\delta_{CM}(1)$ and $\delta_{CM}(3)$ are again shown by arrows.

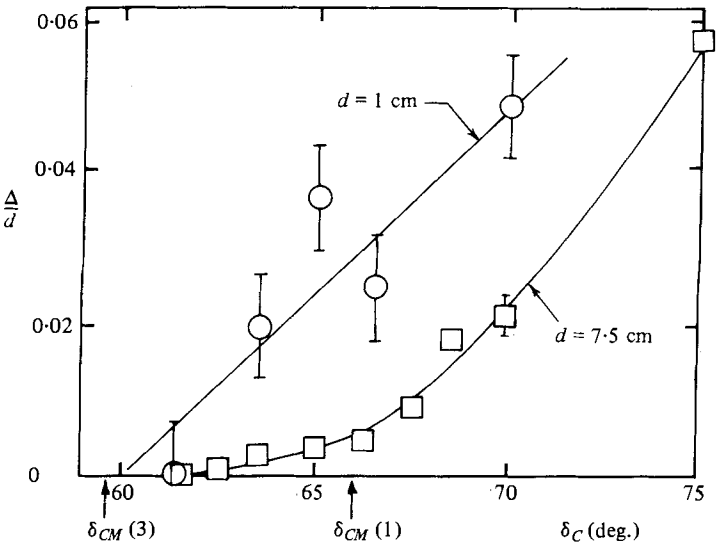

FIGURE 13. Results of dissociating carbon dioxide flows.
○, d = 1 cm; □, d = 7·5 cm.

The higher density and refractive index of the gas in the carbon dioxide flow makes it possible to resolve the shock much more sharply. With care in the adjustment of the interferometer it was even possible to see the shock on cones with d = 0·5 cm provided that it was detached. Examples of the interferograms taken in carbon dioxide flows are shown in figure 12 (plate 1).

The results obtained with carbon dioxide are shown in figure 13, in which the points for d = 1 cm and d = 7·5 cm only have been selected. Here, the separation of the two curves is clearly in the same direction as that in figure 9 and the qualitative behaviour is generally as predicted. The points for d = 3 cm fall between the two curves. It can be seen from figure 13 that the position of the two curves in relation to the two arrows ($\delta_{CM}(1)$ and $\delta_{CM}(3)$) is closer to the equilibrium side than in the case of nitrogen (see figure 11). This is as it should be in view of the difference in the relaxation lengths. For example, the case d = 3 cm in nitrogen gives the same l/d as the case d = 1 cm in carbon dioxide. This is part of the reason for the small separation of the curves in figure 11.

5. Conclusions

Experiments to examine shock detachment in relaxing flow with wedge models had the unavoidable problem that end effects are difficult to separate from relaxation effects. The present experiments were successful in eliminating this difficulty by performing the experiments with cones. The results clearly show that the effect, observed by Hornung & Smith (1979) on wedges, that shock detachment occurs more gradually in a relaxing gas than in equilibrium or frozen flow, is also observed in cone flow.

Considerations of a map of the flow into the speed–deflexion plane again allow the effect to be predicted. However, this mapping is considerably more complex in cone flow, because the conditions after a conical shock are not uniform even in frozen or

equilibrium flow. The speed–deflexion plane map gives a good explanation of the qualitative behaviour of the sonic surface in the flow field as the cone semi-angle is increased.

The experiments were performed with sets of cones of various base diameters, thus varying the parameter l/d without changing the gas. Though the predicted effect was clearly observed in carbon dioxide flows, the limits of resolution of optical interferometry caused the results obtained in nitrogen to be barely significant. As a check, a perfect-gas argon experiment showed the effect to be absent in frozen flow.

The facility used in this project received support from the Australian Research Grants Committee.

REFERENCES

DORRANCE, W. H. 1962 *Viscous Hypersonic Flow*. McGraw-Hill.
EMUNDS, H. 1976 *Deutsche Luft- und Raumfahrt*, DLR-FB 76–26.
HAYES, W. D. & PROBSTEIN, R. F. 1959 *Hypersonic Flow Theory*. Academic.
HORNUNG, H. G. & SMITH, G. H. 1979 *J. Fluid Mech.* **93**, 225.
HORNUNG, H. G. 1977 *Proc. 6th Austral. Hydr. Fluid Mech. Conf. Adelaide*, p. 217.
SOLOMON, G. E. 1955 *N.A.C.A. Rep.* 1242.
VAN DRIEST, E. R. 1952 *N.A.C.A. Tech. Note* 2597.
WALZ, A. 1966 *Strömungs- und Temperaturgrenzschichten*. Braun.
WARD, L. C. & PUGH, P. G. 1968 *A.I.A.A. J.* **6**, 2018.

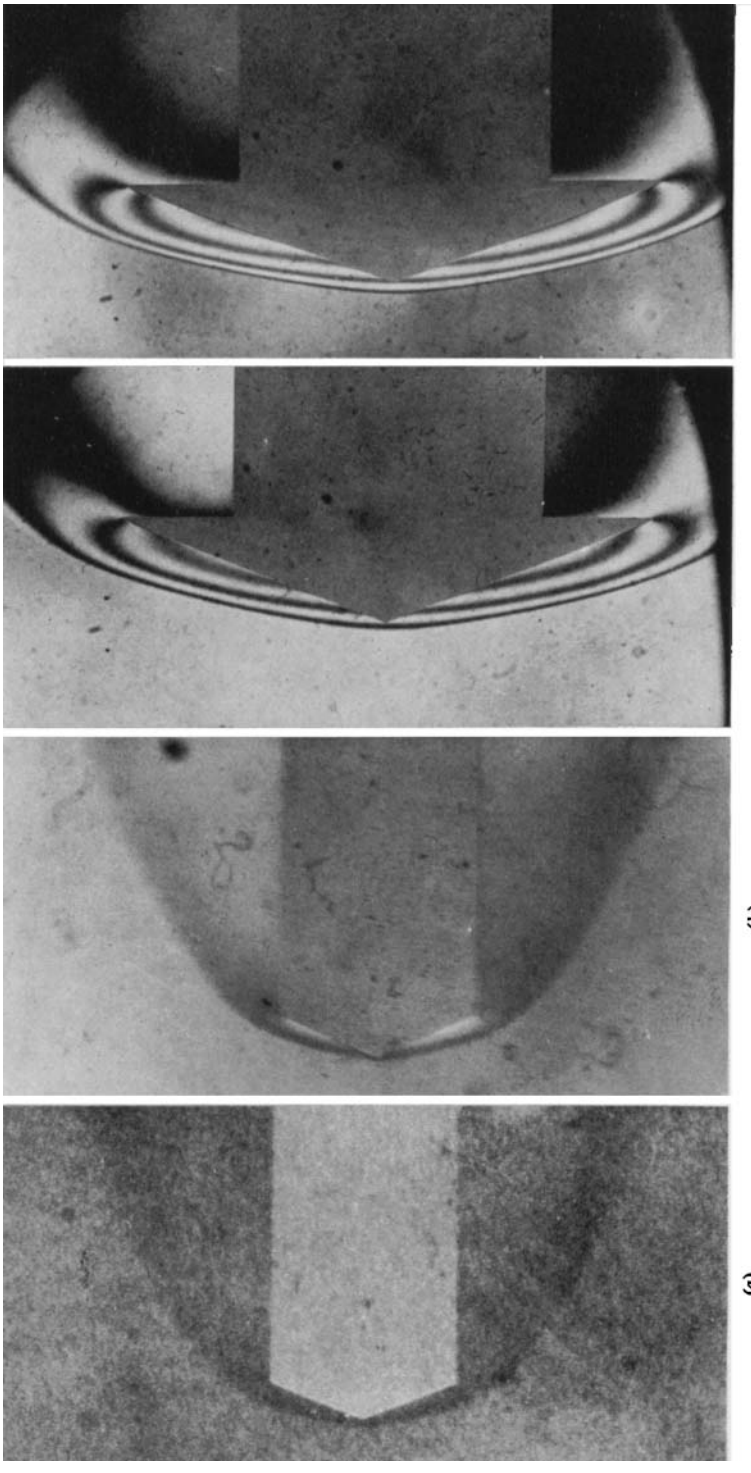

FIGURE 12. Examples of interferograms of dissociating carbon-dioxide flow over cones (*a*) $d = 0{\cdot}5$ cm, $\delta_C = 68{\cdot}5°$; (*b*) $d = 1$ cm, $\delta_C = 65°$; (*c*) $d = 7{\cdot}5$ cm, $\delta_C = 68{\cdot}8°$; (*d*) $d = 7{\cdot}5$ cm, $\delta_C = 70°$.